ORIGINAL RESEARCH

American Society of Plant Biologists · S·E·B SOCIETY FOR EXPERIMENTAL BIOLOGY · WILEY

Nonpolar residues in the presumptive pore-lining helix of mechanosensitive channel MSL10 influence channel behavior and establish a nonconducting function

Grigory Maksaev | Jennette M. Shoots | Simran Ohri | Elizabeth S. Haswell [iD]

Department of Biology and Center for Engineering MechanoBiology, Washington University in Saint Louis, Saint Louis, Missouri

Correspondence
Elizabeth S. Haswell, Department of Biology and Center for Engineering MechanoBiology, Washington University in Saint Louis, One Brookings Drive, Saint Louis, MO 63130.
Email: ehaswell@wustl.edu

Present address
Grigory Maksaev, Department of Cell Biology and Physiology and Center for the Investigation of Membrane Excitability Diseases, Washington University School of Medicine, Saint Louis, MO.

Abstract

Mechanosensitive (MS) ion channels provide a universal mechanism for sensing and responding to increased membrane tension. MscS-like (MSL) 10 is a relatively well-studied MS ion channel from *Arabidopsis thaliana* that is implicated in cell death signaling. The relationship between the amino acid sequence of MSL10 and its conductance, gating tension, and opening and closing kinetics remains unstudied. Here, we identify several nonpolar residues in the presumptive pore-lining transmembrane helix of MSL10 (TM6) that contribute to these basic channel properties. F553 and I554 are essential for wild type channel conductance and the stability of the open state. G556, a glycine residue located at a predicted kink in TM6, is essential for channel conductance. The increased tension sensitivity of MSL10 compared to close homolog MSL8 may be attributed to F563, but other channel characteristics appear to be dictated by more global differences in structure. Finally, MSL10 F553V and MSL10 G556V provided the necessary tools to establish that MSL10's ability to trigger cell death is independent of its ion channel function.

KEYWORDS
Arabidopsis thaliana, electrophysiology, mechanosensitive ion channel, MscS-Like10

1 | INTRODUCTION

The ability to respond to mechanical stimuli is an ancient and intrinsic property of cells (Anishkin, Loukin, Teng, & Kung, 2014; Booth, Miller, Müller, & Lehtovirta-Morley, 2015). One of the most universal mechanisms for mechanotransduction is the use of mechanosensitive (MS) ion channels. MS channels are oligomeric protein structures embedded in the lipid bilayer, and their primary function is to form a conductive pore in response to increased lateral membrane tension or force transduced from cytoskeletal filaments (Bavi et al., 2017). MS channels mediate the perception of external mechanical stimuli (touch, gravity, vibration) and internal mechanical stresses in plants,

animals, and bacteria (Basu & Haswell, 2017; Martinac et al., 2014; Ranade, Syeda, & Patapoutian, 2015). Mammalian MS channel dysfunctions are associated with numerous pathologies (Gu & Gu, 2014) and both mammalian and bacterial MS channels are under investigation as drug targets (Boulos, 2013; Gottlieb, Suchyna, Ostrow, & Sachs, 2004; Iscla et al., 2015). It is therefore important for both basic and applied reasons to determine the molecular mechanisms of MS ion channel function, including the relationship between channel structure and its conductance, gating tension, and opening and closing kinetics.

We already have considerable insight into these questions, in part due to decades of research into the structure and function of a MS ion channel from *Escherichia coli*, the Mechanosensitive ion channel of Small conductance (*Ec*MscS). *Ec*MscS is directly opened by

membrane tension (Sukharev, 2002), has a unitary conductance of 1.2 nS in giant *E. coli* spheroplasts (Levina et al., 1999; Martinac, Buechner, Delcour, Adler, & Kung, 1987), and demonstrates a slight preference for anions (1.2-fold to threefold, summarized in [Maksaev & Haswell, 2013; Cox, Wann, & Martinac, 2014)]. The primary physiological function of *Ec*MscS is to promote bacterial survival when subjected to hypoosmotic shock (Boer, Anishkin, & Sukharev, 2011; Levina et al., 1999). *Ec*MscS also shows inactivation behavior whereby sustained tension leads to a nonconductive state of the channel that cannot be opened again until a period of recovery (Akitake, Anishkin, Liu, & Sukharev, 2007; Belyy, Kamaraju, Akitake, Anishkin, & Sukharev, 2010; Edwards, Bartlett, & Booth, 2008; Kamaraju, Belyy, Rowe, Anishkin, & Sukharev, 2011; Vásquez, 2013).

A wealth of structural information on MscS is available, derived from several members of the MscS family from different bacterial species. Crystal structures thought to represent the conducting state of *Ec*MscS or the nonconducting states of MscS from *E. coli*, *Thermoanaerobacter tengcongensis*, and *Helicobacter pylori* (Bass, Strop, Barclay, & Rees, 2002; Lai, Poon, Kaiser, & Rees, 2013; Zhang et al., 2012) have been determined. A cryo-electron micrograph structure of a MscS homolog from *E. coli*, Ynal, has also been reported (Böttcher, Prazak, Rasmussen, Black, & Rasmussen, 2015). These structures reveal that MscS forms a homoheptamer with a transmembrane (TM) domain localized to the inner *E. coli* membrane and a cytoplasmic "vestibule." Each subunit contains an N-terminal domain comprised of three TM helices and a soluble C-terminal domain. The most C-terminal of the TM helices, TM3, lines the permeation pore. It comprises two regions, TM3a and TM3b, which are separated by a distinctive kink at residue G113. Other key residues include L105 and L109, which form the narrowest constriction of the closed or nonconducting pore, and G121, which is thought to be critical to formation of the closed state (Akitake et al., 2007; Bass et al., 2002).

A comparison of the open-state versus closed-state structures suggests that gating involves swinging a tension-sensitive paddle made up of the TM1/TM2 helices and twisting TM3a about G113. This motion allows L105 and L109 to move out of the pore. Mutational analyses support important roles for L105 and L109 (Miller et al., 2003; Rasmussen et al., 2010) and have shown that G104, A106, and G108 play critical roles in channel gating (Anishkin, Akitake, & Sukharev, 2008; Edwards et al., 2005). A single mutation in this region, A106V, locks the channel in an open conformation and was used to obtain the first open-state crystal structure of *Ec*MscS (Wang et al., 2008). Mutating other residues in TM3, such as S114, L118, A120, L123, F127 (Malcolm & Blount, 2015), Q112, and A120 (Boer et al., 2011) has less dramatic impact on channel properties, only modulating its gating and inactivation kinetics. However, changing the kink-forming residue G113 to alanine prevents inactivation and in combination with G121A severely alters channel opening and closing (Akitake et al., 2007). Residues F68 and L111 may form a force-transmitting clutch between TM2 and TM3, transmitting membrane tension sensed by the TM1/TM2 paddle to the pore-forming TM3 (Belyy, Anishkin, Kamaraju, Liu, & Sukharev, 2010). Surprisingly,

the channel's weak ion selectivity is governed by its cytoplasmic cage, rather than the pore-lining TM3 (Cox et al., 2013; Gamini, Sotomayor, Chipot, & Schulten, 2011). In summary, a combination of modeling and functional assays now provide a general understanding of the conformational changes that ultimately result in channel gating for *Ec*MscS (Booth & Blount, 2012; Martinac et al., 2014; Naismith & Booth, 2012).

These insights into the structural basis of *Ec*MscS mechanosensitivity provide a strong foundation for studying homologs of *Ec*MscS, which are found in all kingdoms of life (Booth et al., 2015; Cox, Nakayama, Nomura, & Martinac, 2015; Haswell, 2007; Martinac & Kloda, 2003; Pivetti et al., 2003). The domain conserved among all these MscS family members is limited to the pore-lining helix and about 100 amino acids of the following soluble domain. The number of predicted transmembrane domains and the structure of N and C termini are highly variable. The channel behavior and physiological function of multiple *Ec*MscS homologs from other bacterial species, archaea, fission yeast, green algae, and land plants have been reported (Çetiner et al., 2017; Hamilton et al., 2015; Kloda & Martinac, 2001; Lee et al., 2016; Maksaev & Haswell, 2012; Malcolm et al., 2012; Nakayama, Fujiu, Sokabe, & Yoshimura, 2007; Nakayama, Yoshimura, & Iida, 2012, 2013). These channels are all mechanically gated and generally function in hypoosmotic stress relief, but have a range of conductances and ion channel selectivities and play different physiological and developmental roles.

The ten *Ec*MscS homologs encoded in the genome of the model land plant *Arabidopsis thaliana* have been named MscS-like or MSL channels (Haswell, 2007). MSL proteins exhibit diverse tissue expression patterns, subcellular localizations, and domain structures (Basu & Haswell, 2017). To date, MSL1, MSL8, and MSL10 are the best-characterized MSLs in terms of ion channel physiology. All three provide tension-gated ion channel activities in native plant cells (Haswell, Peyronnet, Barbier-Brygoo, Meyerowitz, & Frachisse, 2008) and/or when expressed in heterologous systems (Hamilton et al., 2015; Lee et al., 2016; Maksaev & Haswell, 2012). MSL1 is localized to the mitochondrial inner membrane (Lee et al., 2016), while MSL8 and MSL10 are primarily localized to the plasma membrane (Hamilton et al., 2015; Haswell et al., 2008). The unitary conductances of MSL8 and MSL10 expressed in *Xenopus* oocytes are approximately 60 pS and 105 pS, respectively (compare to 340 pS for *Ec*MscS expressed in oocytes) (Hamilton & Haswell, 2017; Hamilton et al., 2015; Maksaev & Haswell, 2011, 2012). MSL8 and MSL10 have a slightly higher preference for anions ($P_{Cl}:P_{Na}$ = 5.6–6.3) than *Ec*MscS. Another intrinsic feature of an MS ion channel is its tension sensitivity, defined as the amount of tension applied to the membrane required for channel opening. The tension at which a channel opens may or may not be the same as the tension at which it closes. Different opening and closing tensions lead to an asymmetric gating profile, and this phenomenon is referred to as hysteresis. Both MSL10 and MSL8 have lower tension sensitivity than *Ec*MscS, and both exhibit strong hysteresis, with much higher opening than closing pressures (Hamilton et al., 2015; Maksaev & Haswell, 2012). We interpret this to mean that, once opened, MSL8 and MSL10 are

very stable and do not close until most of the tension is relieved (Maksaev & Haswell, 2012).

In terms of physiological function, MSL8 appears to serve in a role analogous to that of EcMscS, as it protects pollen from multiple hypoosmotic challenges associated with pollen development and function (Hamilton et al., 2015). MSL8 is primarily localized to the plasma membrane of pollen grains, where it is required for full survival of rehydration, germination, and tube growth. Two mutations in the presumptive pore-lining helix of MSL8, I711S and F720L, alter channel behavior and fail to complement these mutant phenotypes (Hamilton & Haswell, 2017). These observations link ion flux through the MSL8 channel to protection from osmotic stresses during pollen development.

Much less clear is the functional role of MSL10. MSL10 is required for the predominant MS ion channel activity in root cells (Haswell et al., 2008), but to date no other loss-of-function phenotype has been established. Fortunately, gain-of-function phenotypes have been revealing; overexpression of MSL10 leads to cell death, as does a single ethyl methanesulfonate-induced point mutation in the MSL10 C terminus, S640L (rea1) (Veley et al., 2014; Zou et al., 2016). Overexpression of the soluble N terminus of MSL10 is sufficient to induce cell death in tobacco epidermal cells (Veley et al., 2014). Thus, all existing data suggest that MSL10 is a multifunctional MS ion channel that is capable of mediating adaptation to hypoosmotic shock in the short term (reducing pressure by releasing osmolytes) and of signaling to change cellular state in the long-term (inducing cell death in response to biotic or abiotic stress). However, more structural information about MSL proteins and their pore-forming region is required to fully and directly test the possibility that MSL10 has a nonconducting function.

To gain additional information about the structure of the channel pore, the mechanism of gating, and how ion flux through the channel is related to its genetic functions, we used mutational analysis and single-channel patch-clamp electrophysiology to identify residues in the presumptive pore-lining domain of MSL10 that are important for channel behavior, including tension sensitivity, conductivity, and stability of the open state. We then tested two tension-insensitive mutants for the ability to induce cell death in a previously established transient expression assay. These data provide critical information about the structural component of tension-sensitive ion transport and a useful comparison to EcMscS and other MS channels in animals and bacteria. In addition, these mutant MSL10 channels provide tools for studying the relationship between tension sensitivity, open-state stability, ion flux, and cell death signaling.

2 | METHODS

2.1 | Molecular biology

All construct were based on pOO2-MSL10 (Maksaev & Haswell, 2012). Site-directed mutagenesis was used to introduce point mutations into the MSL10 sequence and confirmed by sequencing. Capped RNA was transcribed in vitro with SP6 polymerase using the mMessenger mMachine kit (Ambion, Thermo Fisher Scientific) and stored at −80°C at approximately 1000 ng/μl.

2.2 | Oocyte preparation

Xenopus laevis oocytes (Dumont stage V or VI) were purchased (Ecocyte Bioscience US LLC, Austin, Texas) and handled as described (Maksaev & Haswell, 2015). Oocytes were injected with 50 nl of 1000 ng/μl of RNA the day after isolation. Fluorescent imaging of the oocytes was carried out 48–72 h after injection. Oocytes were mounted on concave slides and covered with coverslips. Confocal imaging of the periphery of the oocytes was performed using Olympus Fluoview 1000 with BX61 microscope and the Olympus FV10-ASW software suite.

2.3 | Electrophysiology

The buffer used was 60 mM $MgCl_2$, 5 mM HEPES, adjusted to pH 7.38 with TEA-OH. All the traces presented were obtained from excised inside-out patches. Data were acquired using an Axopatch 200B amplifier and a Digidata 1440A digitizer (Molecular Devices) at 20 kHz and low-pass filtered at 5 kHz. Channels were activated by symmetric 5-s pressure ramps. Pressure was applied and monitored with a HSPC-1 high speed pressure clamp system (ALA Scientific Instruments), and traces analyzed with Clampfit 10.6 (Molecular Devices). Patch pipettes of approximately the same resistance (3.00 ± 0.25 MOhm) were used in all experiments. The gating threshold of a channel variant was defined as the pressure at which the second channel of the population in a patch opened. For each patch, several pressure ramps of −30 mmHg were run to accommodate for patch creep. Only after that, measurements at −20 mV membrane were performed. For each patch, the results of 7–12 consecutive pressure ramps were averaged. The number of channels per patch was estimated from the peak current at patch rupturing pressure. In cases when the number of open channels was 100 or more, the correction for series pipette resistance was introduced. For closing pressures, the average was taken only in cases when closing pressure was not zero. In case when at least one pull for a patch resulted in at least one open channel after the pressure was released, the closing pressure was considered to be zero.

2.4 | Software

The putative structure of AtMSL10 TM6 (Figure 1b) was obtained from the I-TASSER prediction server (Zhang, 2008) using the EcMscS closed-state crystal structure [2OAU:A, (Bass et al., 2002; Steinbacher, Bass, Strop, & Rees, 2007)] as a template. Sequence alignments and analyses were made using the Unipro UGENE bioinformatics toolkit (Okonechnikov, Golosova, & Fursov, 2012). Visualization of crystal structures and imaging of the putative MSL10 pore region were performed in the VMD suite (Humphrey, Dalke, & Schulten, 1996). Secondary structure of MSL10 was predicted using ARAMEMNON plant membrane protein database (Schwacke et al., 2003).
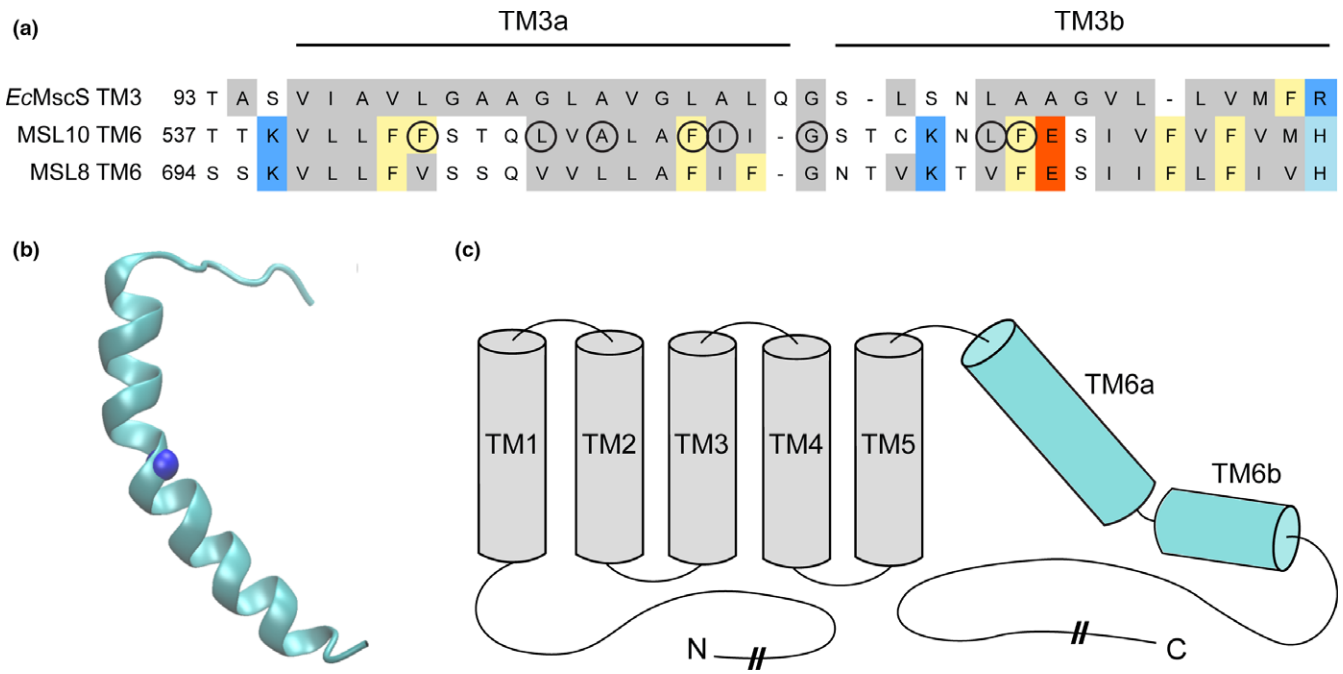
FIGURE 1 Identification of potential pore-disrupting residues in MSL10. (a) Alignment of the pore-lining domain of *Escherichia coli* MscS and corresponding regions of *Arabidopsis thaliana* MSL10 and MSL8. Acidic residues are indicated in red; basic residues in blue; and nonpolar in gray. Phe residues are marked yellow. Circles indicate residues that were analyzed in this report. (b) Side view of the predicted structure of the MSL10 TM6, created with I-TASSER. The side chain at G556, predicted to form a kink, is indicated with a blue sphere. (c) Predicted topology of MSL10, indicating soluble N- and C-termini and six membrane-spanning helices. The lengths of the N- and C-termini are not to scale

2.5 | Cell death assays

The coding sequences of wild-type MSL10, MSL10 F553V, and MSL10 G556V were amplified from the pOO2 vectors described above and cloned into the pK7FWG2 vector for C-terminal GFP tagging and transient expression in *Nicotiana benthamiana* leaves under the control of the 35S promoter. To quantify the amount of dead versus viable epidermal pavement cells, leaves were dual stained with fluorescein diacetate (FDA) and propidium iodide (PI) 5 days after infiltration as described in (Garabagi, Gilbert, Loos, McLean, & Hall, 2012) and visualized via confocal microscopy. As previously outlined, cells were considered dead (i) if their nucleus was stained by PI and/ or (ii) their vacuole disappeared, which is apparent when cytoplasmic FDA/GFP signal fills the entire body of the pavement cell (Veley et al., 2014). In this study, we added a third criterion whereby cells were also considered dead if their vacuole had mostly, though not completely, disappeared. The percentage of cell death reported was the average of four separate infiltration experiments, each consisting of three to four leaves per construct, with $n \sim 60$ cells imaged per leaf.

3 | RESULTS

3.1 | Selection of potential pore-disrupting residues

To identify residues likely to be important for MSL10 ion channel activity, we performed a sequence alignment between the region of highest homology between *Ec*MscS, MSL10, and MSL8 (Figure 1a). In the *Ec*MscS crystal structure, this sequence forms transmembrane (TM) helix 3, the domain that lines the channel pore (Bass et al., 2002). *Ec*MscS TM3 is 33 amino acids long and has a pronounced kink at G113 that splits it into TM3a and TM3b. The analogous sequence in MSL10 is its most C-terminal TM helix, TM6. We therefore generated a hypothetical structure of TM6 using the I-TASSER prediction server (Zhang, 2008) and the *Ec*MscS closed-state crystal structure (2OAU:A (Bass et al., 2002; Steinbacher et al., 2007)), as a template (Figure 1b). These data, along with a topology prediction from the ARAMEMNON server (Schwacke et al., 2003), support the overall topology for MSL10 shown in Figure 1c. Based on this alignment, we identified four key classes of residues within the TM6 sequence that were likely to contribute to MSL10 channel function: (i) multiple phenylalanine residues, (ii) the putative glycine kink, (iii) several nonpolar TM6 residues that differ between MSL10 and MSL8, and (iv) an isoleucine residue known to play a role in MSL8 function. Those residues selected for study are indicated with circles in Figure 1a.

3.2 | Phenylalanine 553 maintains channel conductance and the stability of the open state

One distinction between the amino acid sequences of *Ec*MscS TM3 and MSL10 TM6 is the presence or absence of multiple phenylalanine residues. *Ec*MscS TM3 contains only one Phe residue, and it is located at very end of TM3b. MSL10 has six Phe residues scattered through the pore-lining domain. MSL8 has six Phe residues in its

MAKSAEV ET AL.

American Society
of Plant Biologists
Cultivating a better future through plant biology research

SEB
SOCIETY FOR EXPERIMENTAL BIOLOGY

WILEY

5

TM6; five of these are conserved with MSL10 (indicated in yellow, Figure 1c), and F720 is essential for channel function (Hamilton & Haswell, 2017). To determine whether Phe residues in TM6 are also critical for MSL10 channel function, we used site-directed mutagenesis to change F544, F553, and F563 to smaller nonpolar residues, and to introduce a series of increasingly disruptive changes at F553. We introduced F544V, F553W, F553L, F553V, and F563L mutations into the MSL10 coding sequence of pOO2-MSL10-GFP, and pOO2-MSL10 for in vitro capped RNA (cRNA) production (Maksaev & Haswell, 2012). cRNA for all variants was injected into Xenopus oocytes for expression and characterization as previously described (Maksaev & Haswell, 2015).

To determine whether these mutations affected protein folding or stability, we monitored the trafficking of MSL10 variants fused to GFP by confocal microscopy. All variants produced similar signal at the oocyte periphery 5 days after injection, while no signal was present in water-injected oocytes (Figure 2a). Single-channel patch-clamp electrophysiology was then used to assess the channel behavior (single channel conductance, open-state stability, and tension sensitivity) of each of these MSL10 variants, as in (Maksaev & Haswell, 2015). Current traces from excised inside-out patches derived from oocytes expressing wild type MSL10 showed the expected stable single-channel openings (119.4 ± 4.0 pS at −100 mV, Figure 2b, top). MSL10 F544V did not appear different from the wild type channel. However, MSL10 F553W, MSL10 F553L, and MSL10

F563L exhibited "flickery" channel activity, defined here as rapid increases and decreases in conductance without a clear time spent in the open state (middle and bottom, Figure 2b). We were unable to detect any channel activity in oocytes expressing MSL10 F553V.

We measured the unitary currents produced by MSL10 and MSL10 Phe variant channels under transmembrane potential from 0 to −200 mV. The unitary conductances of MSL10 F544V (114.8 ± 4.0 pS), F553W (121.8 ± 4.3 pS) and F563L (117.7 ± 5.4 pS), calculated at −100 mV membrane potential, were indistinguishable from wild type MSL10 (Figure 2c, Table 1). However, MSL10 F553L produced single-channel currents that were significantly lower than that of the wild type at every voltage tested (Figure 2c), and its conductance at −100 mV was 78.0 ± 4.4 pS, 0.6-fold that of the wild type (Table 1). As noted above, MSL10 F553V did not produce any activity. Thus, successively reducing the bulkiness of residues at position 553 resulted in successively lower unitary channel conductance (W≈F>L>V). We conclude that F553 and F563 both play important roles in maintaining the stability of the open state of MSL10, while F553 also controls channel conductance.

3.3 | Glycine 556 is a key residue for MSL10 channel function

The next residue in MSL10 we chose to investigate was G556. MSL10 G556 aligns with the kink-forming residue G113 in EcMscS (Figure 1a)
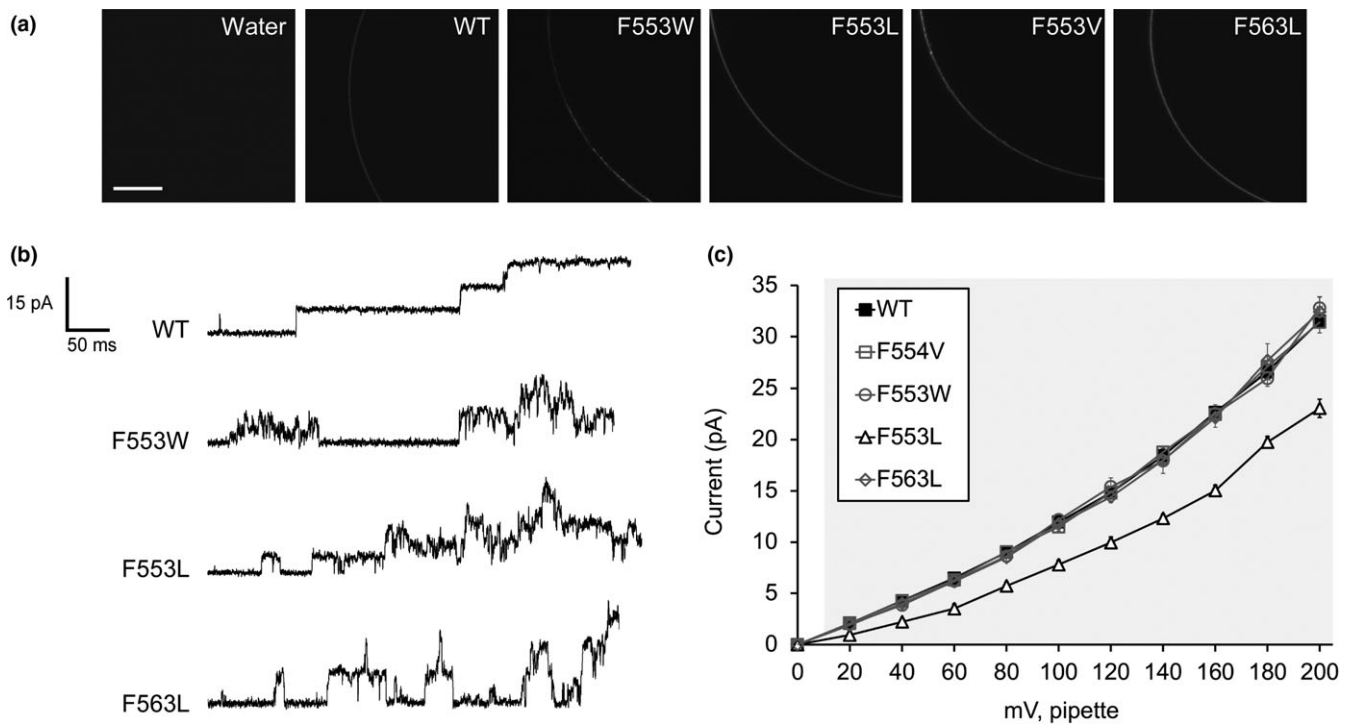
FIGURE 2 Mutagenesis of two TM6 phenylalanines reveals a role for bulky nonpolar residues in maintaining channel conductance and the stability of the open state. (a) Portions of the oocyte periphery 5 days after injection with the indicated MSL10-GFP variant cRNA. Scale bar is 100 μm. (b) Examples of traces at −100 mV membrane potential. 0.5-s fragments of 5-s records of channel activation by symmetric pressure ramps are shown. (c) Current/voltage curves for the indicated MSL10 variants. Each data point is the average current from 3 to 9 patches in 60 mM MgCl$_2$, 4 mM HEPES. Error bars indicate standard deviation but are obscured by the symbols. Gray background indicates voltages where the current produced by MSL10 F553L differed significantly from wild-type MSL10, $p < 0.001$ (Student's t test)

**TABLE 1** Properties of the *At*MSL10 TM6 mutants. Conductance at −100 mV

	Mutation	Conductance at −100 mV	Conductance compared to WT	Open state	Gating characteristics	Cell death
MSL10 WT	None	119.4 ± 4.0 pS	1.0 WT	Stable	Strong hysteresis	Strong
Phe residues	F544V	114.8 ± 4.0 pS	1.0 WT	Stable		
	F553W	121.8 ± 4.3 pS	1.0 WT	Slight flicker		
	F553L	78.0 ± 4.4 pS	0.65 WT	Slight flicker	No hysteresis	
	F553V	N/A	N/A	N/A	N/A	Strong
	F563L	117.7 ± 5.4 pS	1.0 WT	Stable	High gating threshold No hysteresis	
Putative Gly kink	G556A	106.0 ± 4.4 pS	0.9 WT	Stable		
	G556V	N/A	N/A	N/A	N/A	Strong
Change to MSL8	L548V	114.3 ± 5.0 pS	1.0 WT	Stable		
	A550L	112.7 ± 4.6 pS	1.0 WT	Stable		
	L562V	119.2 ± 6.1 pS	1.0 WT	Stable	High gating threshold	
	I554V	121.8 ± 8.1 pS	1.0 WT	Stable		
	I554S	61.1 ± 4.9 pS	0.5 WT	Flickery		Strong

and is predicted to sit at a similar kink in TM6 (Figure 1b). To determine whether G556 plays a role in MSL10 channel function, we changed this residue to the larger nonpolar residues alanine (G556A) or valine (G556V). While both MSL10 variants were expressed in Xenopus oocytes and trafficked normally to the plasma membrane (Figure 3a), neither functioned like the wild type. The MSL10 G556A mutant was active and produced a relatively stable channel opening (Figure 3b). However, it had a unitary conductance of 106.0 ± 4.4 pS, 0.9-fold that of the wild-type channel (Figure 3c). MSL10 G556V did not produce any activity even under extreme membrane tensions and high membrane potentials. Thus, the G556A substitution produced a modest effect, and G556V completely ablated function, presumably

because of increasing size of the side chains. These results establish that G556 plays a key role in the function of MSL10 and are consistent with the prediction that there is bending at this residue within the helix and that mobility at this site is important for the conformational changes associated with channel opening.

3.4 | Nonpolar TM6 residues that differ between MSL10 and MSL8 are not required for wild-type conductance and open-state stability

Nonpolar residues in MSL10 TM6 that are not conserved in MSL8 include F544, L548, A550, I555, and L562. To determine
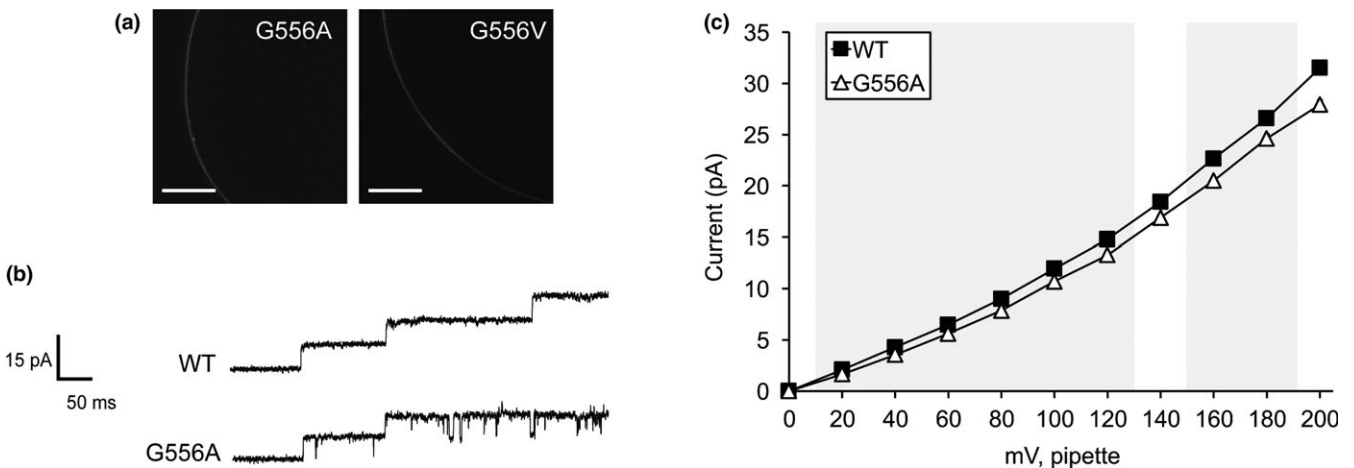
FIGURE 3 Replacing G556 with larger nonpolar residues reduces or ablates channel conductance. (a) Portions of the oocyte periphery 5 days after injection with the indicated MSL10-GFP variant cRNA. Scale bar is 100 μm. (b) Examples of traces at −100 mV membrane potential. 0.5-s fragments of 5-s records of channel activation by symmetric pressure ramps are shown. (c) Current/voltage curves for wild type and MSL10 G556A. Each data point is the average current from 3 to 9 patches in 60 mM MgCl$_2$, 4 mM HEPES. Error bars indicating standard deviation are present but are obscured by the symbols. Wild-type MSL10 curve is from the same data as in Figure 2c. Gray background indicates voltages where the current produced by MSL10 G556A differed significantly from wild-type MSL10, $p < 0.001$ (Student's t test)
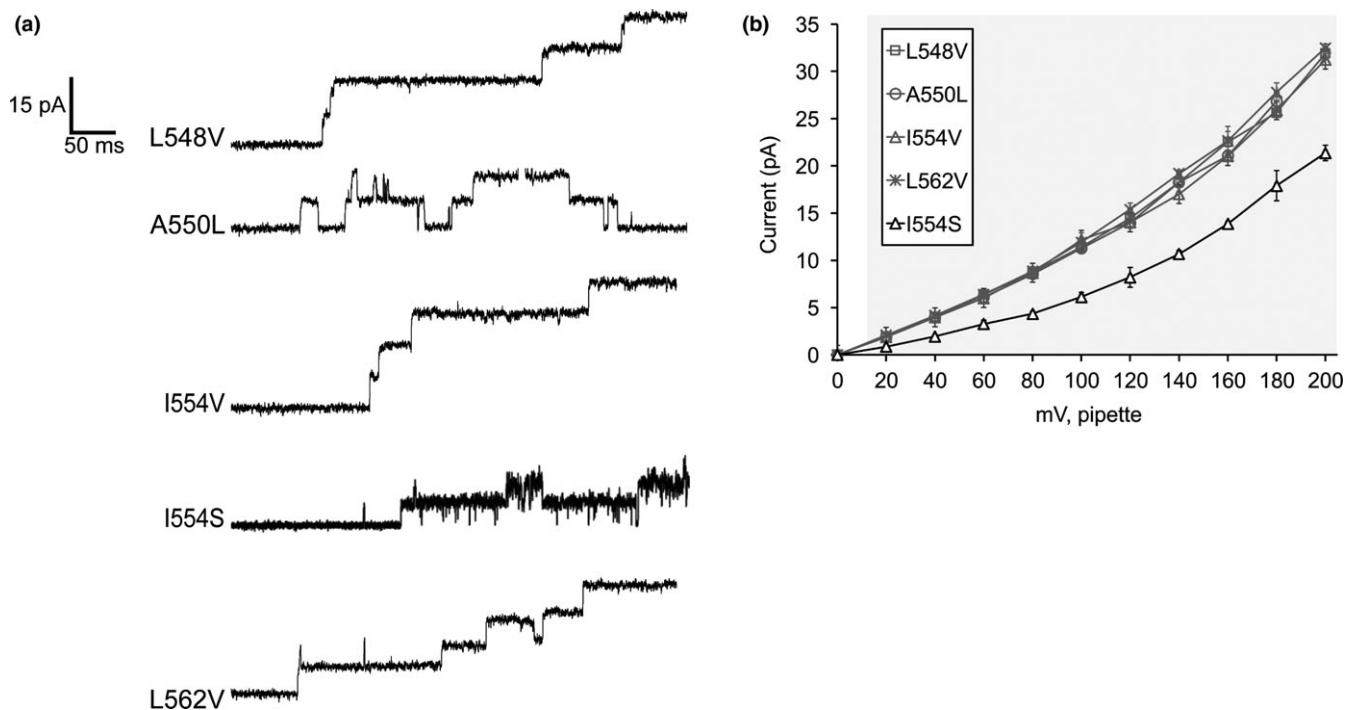
FIGURE 4 Effects of mutating nonpolar residues in TM6 that differ between MSL8 and MSL10. (a) Examples of traces at −100 mV membrane potential. 0.5-s fragments of 5-s records of channel activation by symmetric pressure ramps are shown. (b) Current/voltage curves for the indicated MSL10 variants. L548V, A550L, I554V, and L562V do not differ from the WT. Each data point is the average current from 3 to 9 patches in 60 mM $MgCl_2$, 4 mM HEPES. Error bars indicate standard deviation. Gray background indicates voltages where the current produced by MSL10 I554S differed significantly from wild-type MSL10, $p < 0.001$ (Student's t test)

whether these residues confer the differences in conductance and tension sensitivity between MSL10 and MSL8, we changed several of these residues in MSL10 to the corresponding residue found in MSL8. MSL10 F544V was analyzed with other Phe substitutions in Figure 2 and did not appreciably affect MSL10 channel behavior. MSL10 L548V (114.3 ± 5.0 pS), MSL10 A550L (112.7 ± 4.6 pS), and MSL10 L562V (119.2 ± 6.1 pS) were also indistinguishable from the wild type (119.4 ± 4.0 pS) with respect to unitary conductance and open-state stability (Figure 4a and b, Table 1).

3.5 | Changing isoleucine 554 to serine disrupts channel conductance and the stability of the open state

We previously showed that MSL8 I711S produced a channel with wild-type conductance but an increased tension threshold (Hamilton & Haswell, 2017). We mutated the corresponding residue in MSL10, I554, to valine or serine. While MSL10 I554V exhibited a wild-type unitary conductance (121.8 ± 8.1 pS) and gating pattern, MSL10 I554S was very flickery (Figure 4a), and had a significantly lower unitary conductance than WT (61.1 ± 4.9 pS compared to 119.4 ± 4.0 pS of WT at −100 mV membrane potential, Figure 4b). These unexpected results suggest that MSL10 I554S has normal tension sensitivity, but, has an unstable open state. Taken together, the data shown in Figure 4 suggest that the differences in MSL8 and

MSL10 channel behavior cannot be easily attributed to individual amino acid residues within TM6.

3.6 | Opening and/or closing tension sensitivities were altered in MSL10 F553L, L562V, and F563L

The established approach for measuring tension sensitivity of EcMscS, by calculating the activation midpoint [e.g., refer (Blount, Sukharev, Schroeder, Nagle, & Kung, 1996; Edwards et al., 2005; Maksaev & Haswell, 2011)], is not possible with MSL10 expressed in oocytes, as one typically cannot reach current saturation before the patch collapses (Maksaev & Haswell, 2012). Instead, we measured the gating threshold, or the amount of tension required to open the second channel in the patch. We used pipettes with the same resistance (3.00 ± 0.25 MOhm) to reduce variability in patch size and geometry.

We first analyzed the gating threshold for wild-type MSL10. We observed that the gating threshold depended on the number of channels we observed in a patch prior to saturation or patch rupture and that patches with more channels had a lower opening threshold (Figure 5a). Assuming low open probability and minimal spontaneous gating at zero tension, these data can be fit to a line with slope 0.049 ± 0.02 channels/mm Hg (Figure 5a, circles). The same analyses for MSL10 F553L (squares) and MSL10 L562V (triangles) produced slopes similar to that of the wild type channel, 0.047 ± 0.04 and 0.036 ± 0.01 channels/mm Hg, respectively (Figure 5a).

American Society of Plant Biologists · SEB · WILEY · SOCIETY FOR EXPERIMENTAL BIOLOGY
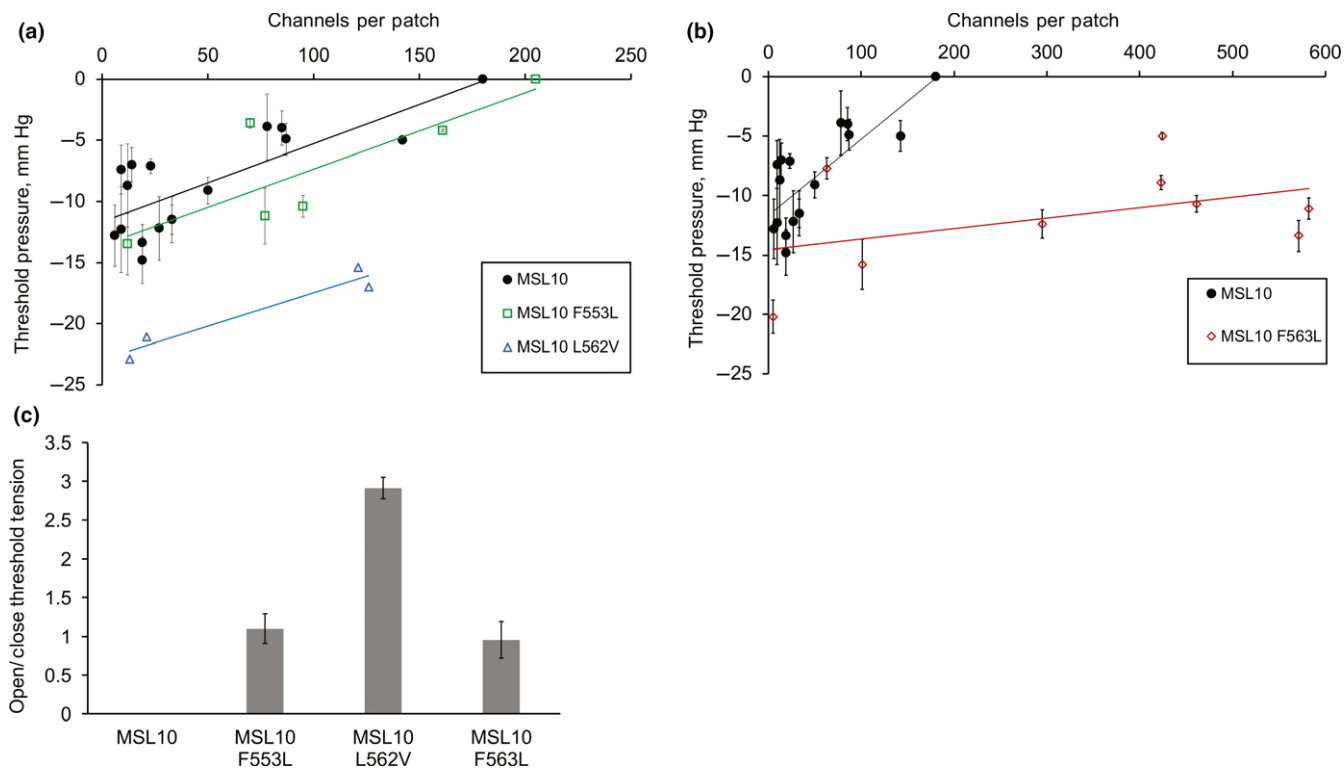
FIGURE 5 Three bulky nonpolar residues affect the threshold tensions of opening and closing. (a, b) Plot of channel number versus threshold tension for wild type MSL10 and the indicated variants. Data were corrected for access resistance. The data for wild-type MSL10 are the same in both plots. Error bars indicate standard deviation between the threshold pressure measured from 5 to 10 trials from a single patch containing the indicated number of channels. (c) The average open/close membrane tension ratios for MSL10 and variants including data from all patches shown in panels a and b. One sample for MSL10 F553L was left out as outlier. Error bars indicate standard deviation between the average open/close ratio for each patch

However, MSL10 F563L did not show a strong dependence of channel number on threshold pressure, with patches containing a range of channel numbers all opening at essentially the same tension. The linear regression line slope for MSL10 F563L was only 0.009 ± 0.007 channels/mm Hg (Figure 5b, diamonds). As shown in Figure 5b, we routinely observed very high channel numbers per patch for MSL10 F563L; in some cases as many as 600 channels per patch.

It is not possible to calculate an open/closed ratio for WT MSL10. In almost every case, one or more channels are still open when all applied tension is released. As a result, the closing threshold tension cannot be calculated. However, the fact that all three MSL10 variants did not show this behavior made it possible to calculate their open/close ratio, using patches with 5–600 channels (Figure 5c). For MSL10 F563L, the open/close ratio was close to one (0.95 ± 0.23). MSL10 L562V had an open/close ratio of 2.9 ± 0.13. For MSL10 F553L, the open/close ratio was close to one (1.10 ± 0.19) when only the four closest data points were considered. A fifth strongly outlying data point was not included, as its value exceeded the upper fence as defined by the quartile method. To summarize, wild-type MSL10 showed threshold opening pressure of around −15 mm Hg and exhibited hysteresis. MSL10 L562V had a high tension threshold for opening but maintained hysteresis. MSL10 F563L had a high tension threshold for both

opening and closing and did not exhibit hysteresis. Due to the small sample size, we can only tentatively conclude that MSL10 F553L lost hysteresis.

3.7 | MSL10 TM6 mutations that ablate channel function do not alter the ability of MSL10 to trigger cell death signaling

These mutations that alter MSL10 channel behavior provide tools to test the structural requirements for MSL10's cell death signaling function. The two MSL10 mutations that produced no ion channel activity (F553V and G556V), along with wild-type MSL10, were fused to GFP and transiently expressed under the strong constitutive cauliflower mosaic virus 35S promoter (35Sp) in tobacco leaf epidermal cells as described previously (Veley et al., 2014). Constructs were coinfiltrated with a plasmid expressing P19 to suppress gene silencing. As shown in Figure 6A, all MSL10 variants were expressed and trafficked normally in tobacco cells. Five days after Agrobacterium infiltration, leaf samples were dual stained for FDA and PI to assess cell death (Figure 6B). As expected, 35% of the cells in leaf samples expressing wild type full-length MSL10 were dead, compared to 14% when P19 was infiltrated alone. Neither MSL10-F553V nor MSL10 G556V produced levels of cell death that were statistically distinguishable from wild type MSL10 (Figure 6C),

FIGURE 6 MSL10 mechanosensitive channel activity is not required for death signaling *in planta*. (a) Localization of MSL10-GFP variants transiently expressed in tobacco epidermal pavement cells. Images were taken 5 days after infiltration. Infiltrations with P19 alone were used as a negative control. Scale bar is 40 μm. Numbers in the lower left-hand corner indicate the voltage setting of the PMT detector when imaging. (b) Examples of cell viability assays. Tobacco leaves expressing MSL10-GFP variants were dual stained with FDA and PI; cells were scored as dead if they had a PI-stained nucleus (indicated by asterisks) or a disappearing vacuole, evidenced by spreading of cytoplasmic signal (arrowhead). Scale bar is 50 μm. (c) Percentage of dead cells quantified from dual staining of 20 leaves (P19 and MSL10) or 10 leaves (MSL10 variants) from multiple infiltration experiments. Error bars indicate standard error. Statistical differences were assessed by one-way ANOVA and Scheffe's test; groups with the same letter did not significantly differ from each other ($p > 0.05$)
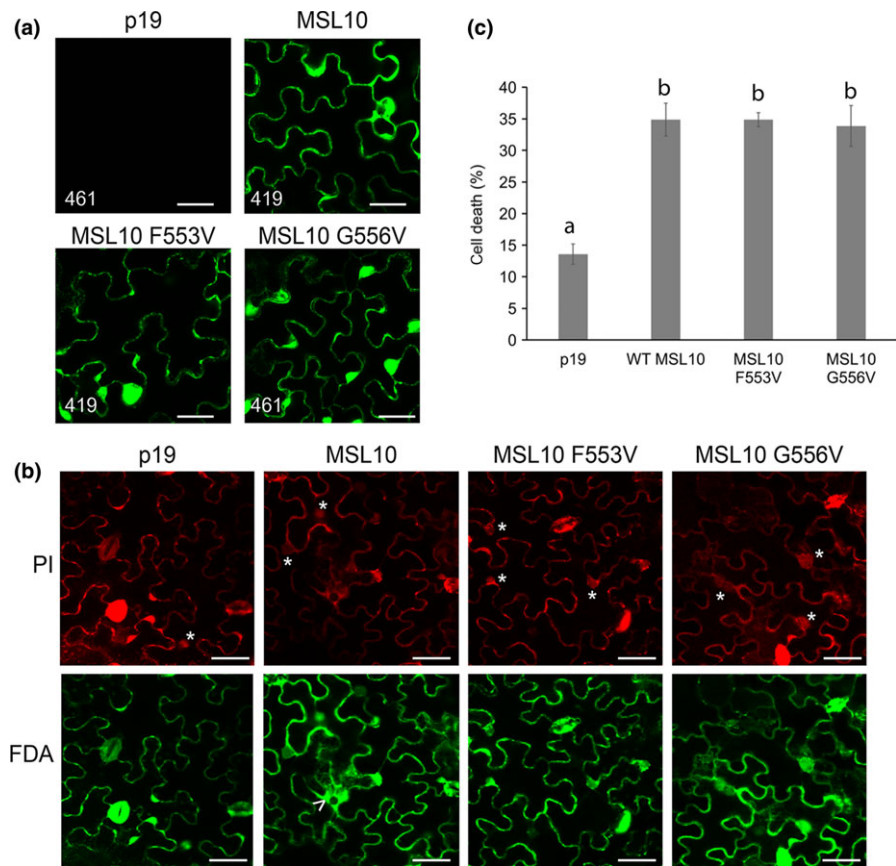
indicating that ion channel function is not required for the ability of full-length MSL10 to trigger cell death in this transient assay.

4 | DISCUSSION

Here, we report the functional effect of twelve different point mutations in the mechanosensitive channel MscS-like (MSL)10 from *Arabidopsis thaliana*. All substitutions were made in a set of eight nonpolar amino acids located in the putative pore-lining transmembrane (TM) helix 6. We observed that four of these mutations (F544V, L548V, A550L, and I554V) did not detectably alter channel behavior in our assays, four primarily affected unitary conductance and/or open-state stability (F553W, F553L, G556A, and I554S), three affected tension sensitivity and/or hysteresis (F553L, L562V, and F563L), and two produced no mechanosensitive channel activity at all (F553V and G556V). Finally, we observed that the latter two variants were as capable as wild type MSL10 of inducing cell death in an *in planta* expression assay.

As Phe residues are found in TM6 of MSL8 and MSL10 but not in TM3 of *Ec*MscS, they were reasonable candidates for residues that underlie the differing channel properties of MSLs and *Ec*MscS. MSL10 has a smaller conductance than *Ec*MscS, and we originally hypothesized that these bigger hydrophobic residues found in the MSL10 TM6 could form a "vapor lock," like *Ec*MscS L105 and L109 (Anishkin & Sukharev, 2004; Bass et al., 2002), or partially obstruct

the channel pore as suggested for F450 in the Arabidopsis SLAC1 channel (Chen et al., 2010). If this were the case, replacing Phe with smaller side chains such as Leu or Val would lead to a deregulated or constitutively open channel. Alternatively, bulky Phe residues could be involved in the slow closing kinetics observed in MSL10 but not in MscS if they participated in a hydrophobic residue-mediated force transduction pathway from the periphery of the channel to its pore, in a manner analogous to the proposed force-transmitting clutch of *Ec*MscS (Belyy et al., 2010). However, none of these hypotheses were correct. Instead, our data suggest that the large hydrophobic nature of the Phe residues at 553 and 563 facilitate the unitary conductance and the stability of the open state of MSL10.

While mutation of F553 to tryptophan had no significant effect on conductance, mutation to leucine led to a decrease in unitary conductance and mutation to valine produced a channel without any apparent mechanosensitive response (Figure 2). Because MSL10 F553L produced a partially functional channel, and because MSL10 F553V was expressed at wild-type levels, MSL10 F553V is likely to produce a stable oligomeric channel that lacks a conductive pore. We thus speculate that the pore size of MSL10 is altered by the size of the side chain at F553; as the side chains at F553 decrease in size, pore-lining domains grow more and more closely packed, thus successively reducing conductance.

While gating pressures for the Phe mutants did not significantly differ from those of WT, both MSL10 F553L and MSL10 F563L

showed almost no hysteresis (Figure 5c). MSL10 typically shows delayed closing relative to opening kinetics; with MSL10 F553L and MSL10 F563L, the ratio of opening and closing tensions was close to 1. This suggested that these mutant channels have an open state that transitions back to the closed state more easily than the wild-type channel. We speculate that the open state is stabilized by interaction between F553 and another hydrophobic residue from the adjacent pore-lining domain of the channel. In this model, the flickery behavior of MSL10 F553L is explained by a steric mismatch between the mutated residue and its interaction partner from the adjacent pore-lining domain. The F553V mutant would have no channel activity as the nonpolar side chain could not create even a partially open pore. There may be a similar interaction that stabilizes the closed state, although F553L has a tension threshold similar to that of the WT MSL10 channel, suggesting that this explanation might be too simple. If reducing the size of the side chain at F553 stabilizes the closed pore, one would expect the flickery F553L channel to be harder to activate. Taken together, the data shown in Figure 2 show that multiple Phe residues in MSL10 TM6 are required for the size and stability of the open pore.

We also found that G556 plays a critical role in MSL10 channel function. We first targeted G556 for mutation because a glycine at a similar position in EcMscS TM3 (G113) has been implicated in gating movements as suggested by crystal structures and molecular dynamics. The EcMscS G113A mutation prevents channel inactivation, presumably by preventing the helix kinking thought to accompany MscS entry from the open state into the inactivated state (Akitake et al., 2007; Boer et al., 2011). While MSL10 does not show inactivation in oocytes [although it does in plant cells (Peyronnet, Tran, Girault, & Frachisse, 2014)], the model for MSL10 TM6 shown in Figure 1 suggests a similar geometry and is consistent with a similar gating movement in the pore-lining helix between MscS and MSL10. We therefore hypothesized that mutations at this site might affect the conformational changes required for channel gating.

While MSL10 G556A showed only a subtle difference from the wild type—a small, but statistically significant, decrease in conductance—MSL10 G556V did not produce any mechanosensitive activity at any applied tensions, though the mutant was expressed at WT levels (Figure 3). We speculate here that the MSL10 G556 side chain faces the pore lumen in the open state and therefore introduction of alanine at position 556 resulted in a decrease in unitary currents (Figure 3b, c). Introduction of the even bigger hydrophobic residue valine at this site might then either fully occlude the channel pore, or prevent the conformational changes associated with channel gating. Whether the same movements are made during the gating transitions of EcMscS and MSL10 is not clear and will certainly require additional experimentation, but the fact that the G556 is a key structural feature of MSL10 TM6 is established.

We addressed the similarities and differences between MSL10 and its close homolog MSL8. We first attempted to link the difference in MSL8 and MSL10 channel characteristics to the differences in the sequence of their putative pore-lining domains. We mutated 3 residues of MSL10 into their counterparts in MSL8, generating

MSL10 L548V, A550L, and L562V (Figure 4). Only the latter had any effect; MSL10 L562V had a high gating threshold (Figure 5a), similar to that previously observed with MSL8 (Hamilton et al., 2015). Thus, L562/V719 may in part be responsible for the difference between MSL8 and MSL10 with respect to tension sensitivity.

We also made mutations in residues conserved between MSL8 and MSL10 that have known effects on MSL8 function. MSL8 I711S exhibited normal conductance but an increased gating threshold and MSL8 F720L was a completely disrupted channel (Hamilton & Haswell, 2017). Analogous mutations altered MSL10 function, but they did not produce the same effects they did in MSL8. MSL10 I554S (aligns with MSL8 I711) produced a flickery channel with half the conductance of the wild type, while MSL10 F563L (aligns with MSL8 F720) produced a channel with normal conductance but an increased gating threshold (Figures 4 and 5). These unexpected results suggest that local or global differences in structure dictate the characteristics of these two channels, so trying to identify individual residues responsible for particular channel characteristics may not be successful.

Residues L562 and F563 form a hydrophobic patch flanked by polar and charged residues (Figure 1a) and our experiments indicate that they are essential for normal tension sensitivity and gating kinetics of the MSL10 channel (Figure 5). Hysteresis is the strongest in WT MSL10, wherein the threshold tension for closing is much lower than for opening. The difference between opening and closing tensions was decreased in MSL10 F562V and completely abolished in MSL10 F563L (Figure 5c). We speculate that these two residues may function as a "force transmitters," similar to L111 of EcMscS TM3. It has been proposed that L111 interacts with F68 from TM2, enabling transduction of the membrane tension into a gating force (Belyy et al., 2010). Similarly, L562 and F563 residues may be a part of an intra-transmembrane helix system that serves to control the closing kinetics of MSL10 by stabilizing the open state.

The concept that ion channels have functions separable from their ability to mediate ion flux (nonconducting functions) is not new and has been established for sodium and potassium channels in animal systems (Feinshreiber et al., 2010; Kruger & Isom, 2016). However, nonconducting functions have not been previously demonstrated for MS ion channels. We previously established that MSL10 is capable of inducing cell death when overexpressed in stable Arabidopsis lines and in transient tobacco expression experiments (Veley et al., 2014). This effect was modulated by seven phosphorylation sites in the soluble N terminus, but these sites did not alter ion channel function, suggesting that the two functions might be separable. Transient overexpression of the soluble N terminus of MSL10 was capable triggering programmed cell death on its own. However, these results left open the possibility that MSL10 ion channel function is required indirectly to activate the cell death signaling mediated by the N terminus and that this effect could be simulated by expressing the truncated, soluble N terminus.

Two of the twelve mutations we tested, MSL10 F553V and MSL10 G556V, were normally expressed and trafficked in Xenopus oocytes but did not exhibit any mechanosensitive ion channel activity

(Figures 2 and 3). These mutants provided the opportunity to test the idea of a nonconducting function for MSL10 more directly and without the caveats of the truncation experiment. The effect of over-expressing these mutant channels did not differ in any way from the wild type, indicating that MS ion channel activity is not required for MSL10's ability to induce cell death in tobacco epidermal cells. The results presented here now firmly establish that MSL10 induces programmed cell death through a mechanism independent of mechanically-induced ion flux. A key future experiment will be to determine whether the nonconducting function of MSL10 is regulated by membrane tension. It will also be worth testing whether nonconducting functions are a conserved feature of proteins in the MscS family, as suggested by a report that the soluble C terminus of MscS interacts with the bacterial fission protein FtsZ (Koprowski et al., 2015).

ACKNOWLEDGMENTS

AUTHOR CONTRIBUTIONS

GM, JMS, and ESH designed experiments and wrote the manuscript; GM, JMS, and SO performed experiments.

ORCID

Elizabeth S. Haswell http://orcid.org/0000-0002-4246-065X

REFERENCES

Akitake, B., Anishkin, A., Liu, N., & Sukharev, S. (2007). Straightening and sequential buckling of the pore-lining helices define the gating cycle of MscS. *Nature Structural & Molecular Biology*, *14*(12), 1141–1149. https://doi.org/10.1038/nsmb1341

Anishkin, A., Akitake, B., & Sukharev, S. (2008). Characterization of the resting MscS: Modeling and analysis of the closed bacterial mechanosensitive channel of small conductance. *Biophysical Journal*, *94*(4), 1252–1266. https://doi.org/10.1529/biophysj.107.110171

Anishkin, A., Loukin, S. H., Teng, J., & Kung, C. (2014). Feeling the hidden mechanical forces in lipid bilayer is an original sense. *Proceedings of the National Academy of Sciences of the United States of America*, *111*(22), 7898–7905. https://doi.org/10.1073/pnas.1313364111

Anishkin, A., & Sukharev, S. (2004). Water dynamics and dewetting transitions in the small mechanosensitive channel MscS. *Biophysics*, *86*(5), 2883–2895. https://doi.org/10.1016/S0006-3495(04)74340-4

Bass, R. B., Strop, P., Barclay, M., & Rees, D. C. (2002). Crystal structure of *Escherichia coli* MscS, a voltage-modulated and mechanosensitive channel. *Science*, *298*(5598), 1582–1587. https://doi.org/10.1126/science.1077945

Basu, D., & Haswell, E. S. (2017). Plant mechanosensitive ion channels: An ocean of possibilities. *Current Opinion in Plant Biology*, *40*, 43–48. https://doi.org/10.1016/j.pbi.2017.07.002

Bavi, N., Nikolaev, Y. A., Bavi, O., Cox, C. D., Qin, Q. H., Martinac, B., & Battle, A. R. (2017). Principles of mechanosensing at the membrane interface. In: R. M. Epand & J.-M. Ruysschaert (Eds.), *The biophysics of cell membranes. Vol 19. Springer series in biophysics* (pp. 85–119). Singapore: Springer. https://doi.org/10.1007/978-981-10-6244-5_4

Belyy, V., Anishkin, A., Kamaraju, K., Liu, N., & Sukharev, S. (2010). The tension-transmitting "clutch" in the mechanosensitive channel MscS. *Nature Structural & Molecular Biology*, *17*(4), 451–458. https://doi.org/10.1038/nsmb.1775

Belyy, V., Kamaraju, K., Akitake, B., Anishkin, A., & Sukharev, S. (2010). Adaptive behavior of bacterial mechanosensitive channels is coupled to membrane mechanics. *Journal of General Physiology*, *135*(6), 641–652. https://doi.org/10.1085/jgp.200910371

Blount, P., Sukharev, S. I., Schroeder, M. J., Nagle, S. K., & Kung, C. (1996). Single residue substitutions that change the gating properties of a mechanosensitive channel in *Escherichia coli*. *Proceedings of the National Academy of Sciences of the United States of America*, *93*(21), 11652–11657.

Boer, M., Anishkin, A., & Sukharev, S. (2011). Adaptive MscS gating in the osmotic permeability response in *E. coli*: The question of time. *Biochemistry*, *50*(19), 4087–4096. https://doi.org/10.1021/bi1019435

Booth, I. R., & Blount, P. (2012). The MscS and MscL families of mechanosensitive channels act as microbial emergency release valves. *Journal of Bacteriology*, *194*(18), 4802–4809. https://doi.org/10.1128/JB.00576-12

Booth, I. R., Miller, S., Müller, A., & Lehtovirta-Morley, L. (2015). The evolution of bacterial mechanosensitive channels. *Cell Calcium*, *57*(3), 140–150. https://doi.org/10.1016/j.ceca.2014.12.011

Böttcher, B., Prazak, V., Rasmussen, A., Black, S. S., & Rasmussen, T. (2015). The structure of YnaI implies structural and mechanistic conservation in the MscS family of mechanosensitive channels. *Structure*, *23*(9), 1705–1714. https://doi.org/10.1016/j.str.2015.06.023

Boulos, R. A. (2013). Antimicrobial dyes and mechanosensitive channels. *Antonie van Leeuwenhoek*, *104*(2), 155–167. https://doi.org/10.1007/s10482-013-9937-x

Çetiner, U., Rowe, I., Schams, A., Mayhew, C., Rubin, D., Anishkin, A., & Sukharev, S. (2017). Tension-activated channels in the mechanism of osmotic fitness in *Pseudomonas aeruginosa*. *Journal of General Physiology*, *149*(5), 595–609. https://doi.org/10.1085/jgp.201611699

Chen, Y.-H., Hu, L., Punta, M., Bruni, R., Hillerich, B., Kloss, B., . . . Hendrickson, W. A. (2010). Homologue structure of the SLAC1 anion channel for closing stomata in leaves. *Nature*, *467*(7319), 1074–1080. https://doi.org/10.1038/nature09487

Cox, C. D., Nakayama, Y., Nomura, T., & Martinac, B. (2015). The evolutionary "tinkering" of MscS-like channels: Generation of structural and functional diversity. *Pflugers Archiv-European Journal of Physiology*, *467*(1), 3–13. https://doi.org/10.1007/s00424-014-1522-2

Cox, C. D., Nomura, T., Ziegler, C. S., Campbell, A. K., Wann, K. T., & Martinac, B. (2013). Selectivity mechanism of the mechanosensitive channel MscS revealed by probing channel subconducting states. *Nature Communications*, *4*, 2137. https://doi.org/10.1038/ncomms3137

Cox, C. D., Wann, K. T., & Martinac, B. (2014). Selectivity mechanisms in MscS-like channels: From structure to function. *Channels (Austin)*, *8*(1), 5–12. https://doi.org/10.4161/chan.27107

Edwards, M. D., Bartlett, W., & Booth, I. R. (2008). Pore mutations of the *Escherichia coli* MscS channel affect desensitization but not ionic preference. *Biophysical Journal*, *94*(8), 3003–3013. https://doi.org/10.1529/biophysj.107.123448

Edwards, M. D., Li, Y., Kim, S., Miller, S., Bartlett, W., Black, S., . . . Booth, I. R. (2005). Pivotal role of the glycine-rich TM3 helix in gating the MscS mechanosensitive channel. *Nature Structural & Molecular Biology*, *12*(2), 113–119. https://doi.org/10.1038/nsmb895

Feinshreiber, L., Singer-Lahat, D., Friedrich, R., Matti, U., Sheinin, A., Yizhar, O., . . . Lotan, I. (2010). Non-conducting function of the Kv2.1

channel enables it to recruit vesicles for release in neuroendocrine and nerve cells. *Journal of Cell Science*, 123(Pt 11), 1940–1947. https://doi.org/10.1242/jcs.063719

Gamini, R., Sotomayor, M., Chipot, C., & Schulten, K. (2011). Cytoplasmic domain filter function in the mechanosensitive channel of small conductance. *Biophysical Journal*, 101(1), 80–89. https://doi.org/10.1016/j.bpj.2011.05.042

Garabagi, F., Gilbert, E., Loos, A., McLean, M. D., & Hall, J. C. (2012). Utility of the P19 suppressor of gene-silencing protein for production of therapeutic antibodies in Nicotiana expression hosts. *Plant Biotechnology Journal*, 10(9), 1118–1128. https://doi.org/10.1111/j.1467-7652.2012.00742.x

Gottlieb, P. A., Suchyna, T. M., Ostrow, L. W., & Sachs, F. (2004). Mechanosensitive ion channels as drug targets. *Current Drug Targets: CNS & Neurological Disorders*, 3(4), 287–295.

Gu, Y., & Gu, C. (2014). Physiological and pathological functions of mechanosensitive ion channels. *Molecular Neurobiology*, 50(2), 339–347. https://doi.org/10.1007/s12035-014-8654-4

Hamilton, E. S., & Haswell, E. S. (2017). The tension-sensitive ion transport activity of MSL8 is critical for its function in pollen hydration and germination. *Plant and Cell Physiology*, 58, 1–16. https://doi.org/10.1093/pcp/pcw230

Hamilton, E. S., Jensen, G. S., Maksaev, G., Katims, A., Sherp, A. M., & Haswell, E. S. (2015). Mechanosensitive channel MSL8 regulates osmotic forces during pollen hydration and germination. *Science*, 350(6259), 438–441. https://doi.org/10.1126/science.aac6014

Haswell, E. S. (2007). MscS-like proteins in plants. In O. P. Hamill (Ed.), *Mechanosensitive ion channels, part A. Vol 58. Current topics in membranes* (pp. 329–359). London: Academic Press.

Haswell, E. S., Peyronnet, R., Barbier-Brygoo, H., Meyerowitz, E. M., & Frachisse, J.-M. (2008). Two MscS homologs provide mechanosensitive channel activities in the Arabidopsis root. *Current Biology*, 18(10), 730–734. https://doi.org/10.1016/j.cub.2008.04.039

Humphrey, W., Dalke, A., & Schulten, K. (1996). VMD: Visual molecular dynamics. *Journal of Molecular Graphics*, 14(1), 33–38, 27–8.

Iscla, I., Wray, R., Blount, P., Larkins-Ford, J., Conery, A. L., Ausubel, F. M., ... Boulos, R. A. (2015). A new antibiotic with potent activity targets MscL. *Journal of Antibiotics*, 68(7), 453–462. https://doi.org/10.1038/ja.2015.4

Kamaraju, K., Belyy, V., Rowe, I., Anishkin, A., & Sukharev, S. (2011). The pathway and spatial scale for MscS inactivation. *Journal of General Physiology*, 138(1), 49–57. https://doi.org/10.1085/jgp.201110606

Kloda, A., & Martinac, B. (2001). Molecular identification of a mechanosensitive channel in archaea. *Biophysics*, 80(1), 229–240. https://doi.org/10.1016/S0006-3495(01)76009-2

Koprowski, P., Grajkowski, W., Balcerzak, M., Filipiuk, I., Fabczak, H., & Kubalski, A. (2015). Cytoplasmic domain of MscS interacts with cell division protein FtsZ: A possible non-channel function of the mechanosensitive channel in *Escherichia coli*. *PLoS ONE*, 10(5), e0127029. https://doi.org/10.1371/journal.pone.0127029

Kruger, L. C., & Isom, L. L. (2016). Voltage-gated Na+ channels: Not just for conduction. *Cold Spring Harbor Perspectives Biology*, 8(6), a029264. https://doi.org/10.1101/cshperspect.a029264

Lai, J. Y., Poon, Y. S., Kaiser, J. T., & Rees, D. C. (2013). Open and shut: Crystal structures of the dodecylmaltoside solubilized mechanosensitive channel of small conductance from *Escherichia coli* and *Helicobacter pylori* at 4.4 Å and 4.1 Å resolutions. *Protein Science*, 22(4), 502–509. https://doi.org/10.1002/pro.2222

Lee, C. P., Maksaev, G., Jensen, G. S., Murcha, M. W., Wilson, M. E., Fricker, M., ... Sweetlove, L. J. (2016). MSL1 is a mechanosensitive ion channel that dissipates mitochondrial membrane potential and maintains redox homeostasis in mitochondria during abiotic stress. *Plant Journal*, 88(5), 809–825. https://doi.org/10.1111/tpj.13301

Levina, N., Tötemeyer, S., Stokes, N. R., Louis, P., Jones, M. A., & Booth, I. R. (1999). Protection of *Escherichia coli* cells against extreme turgor by activation of MscS and MscL mechanosensitive channels: Identification of genes required for MscS activity. *EMBO Journal*, 18(7), 1730–1737. https://doi.org/10.1093/emboj/18.7.1730

Maksaev, G., & Haswell, E. S. (2011). Expression and characterization of the bacterial mechanosensitive channel MscS in *Xenopus laevis* oocytes. *Journal of General Physiology*, 138(6), 641–649. https://doi.org/10.1085/jgp.201110723

Maksaev, G., & Haswell, E. S. (2012). MscS-Like10 is a stretch-activated ion channel from *Arabidopsis thaliana* with a preference for anions. *Proceedings of the National Academy of Sciences of the United States of America*, 109(46), 19015–19020. https://doi.org/10.1073/pnas.1213931109

Maksaev, G., & Haswell, E. S. (2013). Recent characterizations of MscS and its homologs provide insight into the basis of ion selectivity in mechanosensitive channels. *Channels (Austin)*, 7(3), 215–220. https://doi.org/10.4161/chan.24505

Maksaev, G., & Haswell, E. S. (2015). Expressing and characterizing mechanosensitive channels in Xenopus oocytes. *Methods in Molecular Biology*, 1309(Chapter 13), 151–169. https://doi.org/10.1007/978-1-4939-2697-8_13

Malcolm, H. R., & Blount, P. (2015). Mutations in a conserved domain of *E. coli* MscS to the most conserved superfamily residue leads to kinetic changes. *PLoS ONE*, 10(9), e0136756. https://doi.org/10.1371/journal.pone.0136756

Malcolm, H. R., Heo, Y.-Y., Caldwell, D. B., McConnell, J. K., Hawkins, J. F., Guayasamin, R. C., ... Maurer, J. A. (2012). Ss-bCNGa: A unique member of the bacterial cyclic nucleotide gated (bCNG) channel family that gates in response to mechanical tension. *European Biophysics Journal*, 41(12), 1003–1013. https://doi.org/10.1007/s00249-012-0855-z

Martinac, B., Buechner, M., Delcour, A. H., Adler, J., & Kung, C. (1987). Pressure-sensitive ion channel in *Escherichia coli*. *Proceedings of the National Academy of Sciences of the United States of America*, 84(8), 2297–2301.

Martinac, B., & Kloda, A. (2003). Evolutionary origins of mechanosensitive ion channels. *Progress in Biophysics and Molecular Biology*, 82(1–3), 11–24.

Martinac, B., Nomura, T., Chi, G., Petrov, E., Rohde, P. R., Battle, A. R., ... Landsberg, M. J. (2014). Bacterial mechanosensitive channels: Models for studying mechanosensory transduction. *Antioxidants & Redox Signaling*, 20(6), 952–969. https://doi.org/10.1089/ars.2013.5471

Miller, S., Bartlett, W., Chandrasekaran, S., Simpson, S., Edwards, M., & Booth, I. R. (2003). Domain organization of the MscS mechanosensitive channel of *Escherichia coli*. *EMBO Journal*, 22(1), 36–46. https://doi.org/10.1093/emboj/cdg011

Naismith, J. H., & Booth, I. R. (2012). Bacterial mechanosensitive channels—MscS: Evolution's solution to creating sensitivity in function. *Annual Review of Biophysics*, 41(1), 157–177. https://doi.org/10.1146/annurev-biophys-101211-113227

Nakayama, Y., Fujiu, K., Sokabe, M., & Yoshimura, K. (2007). Molecular and electrophysiological characterization of a mechanosensitive channel expressed in the chloroplasts of Chlamydomonas. *Proceedings of the National Academy of Sciences of the United States of America*, 104(14), 5883–5888. https://doi.org/10.1073/pnas.0609996104

Nakayama, Y., Yoshimura, K., & Iida, H. (2012). Organellar mechanosensitive channels in fission yeast regulate the hypo-osmotic shock response. *Nature Communications*, 3, 1020. https://doi.org/10.1038/ncomms2014

Nakayama, Y., Yoshimura, K., & Iida, H. (2013). Electrophysiological characterization of the mechanosensitive channel MscCG in *Corynebacterium glutamicum*. *Biophysical Journal*, 105(6), 1366–1375. https://doi.org/10.1016/j.bpj.2013.06.054

Okonechnikov, K., Golosova, O., & Fursov, M. (2012). UGENE team. Unipro UGENE: A unified bioinformatics toolkit. *Bioinformatics*, 28(8), 1166–1167. https://doi.org/10.1093/bioinformatics/bts091

Peyronnet, R., Tran, D., Girault, T., & Frachisse, J.-M. (2014). Mechanosensitive channels: Feeling tension in a world under pressure. *Front Plant Science*, *5*(204), 558. https://doi.org/10.3389/fpls.2014.00558

Pivetti, C. D., Yen, M. R., Miller, S., Busch, W., Tseng, Y. H., Booth, I. R., & Saier, M. H. Jr (2003). Two families of mechanosensitive channel proteins. *Microbiology and Molecular Biology Reviews*, *67*(1), 66–85. https://doi.org/10.1128/mmbr.67.1.66-85.2003

Ranade, S. S., Syeda, R., & Patapoutian, A. (2015). Mechanically activated ion channels. *Neuron*, *87*(6), 1162–1179. https://doi.org/10.1016/j.neuron.2015.08.032

Rasmussen, T., Edwards, M. D., Black, S. S., Rasmussen, A., Miller, S., & Booth, I. R. (2010). Tryptophan in the pore of the mechanosensitive channel MscS: Assessment of pore conformations by fluorescence spectroscopy. *Journal of Biological Chemistry*, *285*(8), 5377–5384. https://doi.org/10.1074/jbc.M109.071472

Schwacke, R., Schneider, A., van der Graaff, E., Fischer, K., Catoni, E., Desimone, M., . . . Kunze, R. (2003). ARAMEMNON, a novel database for Arabidopsis integral membrane proteins. *Plant Physiology*, *131*(1), 16–26. https://doi.org/10.1104/pp.011577

Steinbacher, S., Bass, R., Strop, P., & Rees, D. C. (2007). Structures of the prokaryotic mechanosensitive channels MscL and MscS. In: O. P. Hamill (Ed.), *Mechanosensitive ion channels, part A. Vol 58. Current topics in membranes* (pp. 1–24). London: Academic Press.

Sukharev, S. (2002). Purification of the small mechanosensitive channel of *Escherichia coli* (MscS): The subunit structure, conduction, and gating characteristics in liposomes. *Biophysical Journal*, *83*(1), 290–298. https://doi.org/10.1016/S0006-3495(02)75169-2

Vásquez, V. (2013). MscS inactivation: An exception rather than the rule. An extremophilic MscS reveals diversity within the family. *Biophysical Journal*, *104*(7), 1391–1393. https://doi.org/10.1016/j.bpj.2013.02.010

Veley, K. M., Maksaev, G., Frick, E. M., January, E., Kloepper, S. C., & Haswell, E. S. (2014). Arabidopsis MSL10 has a regulated cell death signaling activity that is separable from its mechanosensitive ion channel activity. *Plant Cell*, *26*(7), 3115–3131. https://doi.org/10.1105/tpc.114.128082

Wang, W., Black, S. S., Edwards, M. D., Miller, S., Morrison, E. L., Bartlett, W., . . . Booth, I. R. (2008). The structure of an open form of an *E. coli* mechanosensitive channel at 3.45 A resolution. *Science*, *321*(5893), 1179–1183. https://doi.org/10.1126/science.1159262

Zhang, Y. (2008). I-TASSER server for protein 3D structure prediction. *BMC Bioinformatics*, *9*(1), 40. https://doi.org/10.1186/1471-2105-9-40

Zhang, X., Wang, J., Feng, Y., Ge, J., Li, W., Sun, W., . . . Yang, M. (2012). Structure and molecular mechanism of an anion-selective mechanosensitive channel of small conductance. *Proceedings of the National Academy of Sciences of the United States of America*, *109*(44), 18180–18185. https://doi.org/10.1073/pnas.1207977109

Zou, Y., Chintamanani, S., He, P., Fukushige, H., Yu, L., Shao, M., . . . Zhou, J. M. (2016). A gain-of-function mutation in Msl10 triggers cell death and wound-induced hyperaccumulation of jasmonic acid in Arabidopsis. *Journal of Integrative Plant Biology*, *58*(6), 600–609. https://doi.org/10.1111/jipb.12427

SUPPORTING INFORMATION

Additional supporting information may be found online in the Supporting Information section at the end of the article.